Research Square

Preprints are preliminary reports that have not undergone peer review.
They should not be considered conclusive, used to inform clinical practice,
or referenced by the media as validated information.

Visualization Evolution of Higher Alcohols from Direct Conversion of CO_2 on Fe_3O_4-Fe_5C_2-Cu Heterogeneous Catalytic Interfaces Layout

Noritatsu Tsubaki

tsubaki@eng.u-toyama.ac.jp

University of Toyama https://orcid.org/0000-0001-6786-5058

Teng Li

University of Toyama https://orcid.org/0000-0003-3148-643X

Lijun Zhang

Anhui University of Technology https://orcid.org/0000-0002-1958-9404

Zhenkun Liu

University of Toyama

Jiaming Liang

University of Toyama

Hao Chen

University of Toyama

Linlin Zhao

University of Toyama

Shunnosuke Fujii

University of Toyama

Peng Qin

University of Toyama

Qiang Liu

Shandong Energy Group Co., Ltd

Tao Li

Shandong Energy Group Co., Ltd

Tao Xing

Shandong Energy Group Co., Ltd

Jiancai Sui

Shandong Energy Group Co., Ltd

Yongqiang Gu

Shandong Energy Group Co., Ltd

Zhiliang Jin

North Minzu University https://orcid.org/0000-0002-3793-6588

Article

Keywords: Visualization Evolution, Higher Alcohols, CO2-Modified Fischer-Tropsch, Heterogeneous Catalytic Interfaces

Posted Date: April 20th, 2026

DOI: https://doi.org/10.21203/rs.3.rs-9403796/v1

License: This work is licensed under a Creative Commons Attribution 4.0 International License. Read Full License

Additional Declarations: There is **NO** Competing Interest.

Version of Record: A version of this preprint was published at Nature Communications on July 2nd, 2026. See the published version at https://doi.org/10.1038/s41467-026-75201-7.

Abstract

Selective synthesis of alcohols from carbon-based feedstocks remains a fundamental challenge due to complex reaction networks and competing pathways. Here we report a titanium iron ore material FeTiOx synthesized via a high-temperature calcination strategy that introduces amorphous Ti species into the catalyst framework. The FeTiOx system exhibits an intrinsic preference for higher alcohols formation, and tuning the dispersion of Cu species further enhances higher alcohols selectivity to 31.4%, while maintaining a CO2 conversion rate of 42.5%. Operando X-ray diffraction (XRD) and diffuse reflectance Fourier transform infrared spectroscopy (DRIFT) were employed to monitor the evolution of the catalyst phase structure (Fe2O3 → Fe3O4 → Fe5C2) and chemical intermediates (CO, *CHx, CH3CH2O) in real time, thereby elucidating the dynamic evolutions of the catalyst phases and surface intermediates under reaction conditions. These results uncover the structural adaptability of the catalyst and its role in regulating key reaction intermediates. This work highlights the importance of phase-structure engineering in Fe-based catalytic systems and provides a strategy for designing efficient catalysts for selective higher alcohols synthesis.

Introduction

Mounting environmental pressures, driven by escalating CO_2 emissions and the depletion of conventional fossil resources [1-5], demand transformative strategies for sustainable fuel and chemical production. As carbon neutrality becomes an international mandate, catalytic processes capable of valorizing CO_2 into energy-dense molecules have emerged as compelling alternatives [6-10]. In this context, CO_2-modified Fischer-Tropsch synthesis has gained significant attention, as it couples syngas chemistry with carbon-utilization pathways to reshape traditional hydrocarbon formation [11, 12]. By integrating CO_2 activation with tailored catalyst design, this approach offers a promising route toward carbon-circular manufacturing while retaining the versatility of the Fischer-Tropsch platform [13-15].

The accelerating accumulation of atmospheric CO_2 has intensified the urgency of developing catalytic routes capable of transforming this inert molecule into value-added oxygenates. Among these pathways, CO_2-modified Fischer-Tropsch synthesis offers a particularly compelling platform for constructing carbon-efficient processes, especially for the selective formation of higher alcohols [16, 17]. Recent advances highlight the promise of Cu-doped iron catalysts, whose distinctive electronic and structural synergies enhance both CO_2 activation and subsequent C-C coupling [18, 19]. The incorporation of Cu modifies the reducibility and phase evolution of iron species, stabilizes key carbide and oxide intermediates, and promotes hydrogenation-carbonylation equilibria that governs alcohol-chain growth [16, 18, 20, 21]. These cooperative effects lead to more controlled propagation of oxygenated intermediates and improved selectivity toward C_2^+ alcohols. As mechanistic insights into metal-metal and metal-oxide interfaces continue to deepen, Cu-modified iron catalysts are emerging as a central platform for steering CO_2 conversion toward higher alcohols with greater efficiency and precision [22, 23].

Building on these considerations, we successfully synthesized a titanium iron ore material $FeTiO_x$ catalyst through a high-temperature calcination strategy, which enables the formation of amorphous Ti species within the lattice. Catalytic evaluation reveals that this inorganic perovskite exhibits a pronounced selectivity toward alcohol formation during the reaction. By further regulating the dispersion of Cu species on the catalyst surface, the selectivity toward alcohols in products can be significantly enhanced, reaching up to 31.1%. To gain mechanistic insight into the catalytic process, operando XRD and operando DRIFT spectra were employed to real-time monitor the dynamic evolution of the catalyst phase structure and surface intermediates under reaction conditions. These operando measurements provide direct evidence for the formation of Fe_5C_2 and Fe_3O_4 as the active phases, and for the CO-insertion pathway via $*CH_x$ and intermediates, offering a reliable basis for the rational design of selective alcohol synthesis catalysts.

Results

Catalytic Activity

All catalysts were synthesized using a high-temperature calcination strategy (for detailed information, refer to the Supporting Information). Prior to activity testing, each catalyst underwent activation in pure hydrogen gas at 400 °C under atmospheric pressure for 8 h. Subsequently, the activated catalysts were evaluated for the performance in the hydrogenation of CO_2 to produce higher alcohols under conditions of 5.0 MPa, CO_2:H_2 = 1:2.5, and a Gas Hourly Space Velocity (GHSV) of 4800 mL g_{cat}^{-1} h^{-1} (unless otherwise specified). As illustrated in Figure 1a and Supplementary Table 1, the 1%Na-$FeTiO_x$ catalyst exhibits a selectivity of 16.4% (16.1%) for alcohols (higher alcohols) during the CO_2 hydrogenation process, indicating that the presence of amorphous Ti imparts specificity in the directed synthesis of alcohols and higher alcohols from Fe-based catalysts. The introduction of an appropriate amount of Cu further enhances the selectivity of higher alcohols. Figure 1a and Supplementary Table 1 demonstrates that the introduction of an optimal amount of Cu significantly increases the higher alcohols selectivity of the 1%Na-$FeTiO_x$ from 16.4% (16.1%) to 28.0% (26.9%). Notably, the introduction of Cu into the iron-based catalytic system inevitably reduces the CO_2 activation capability while promoting H_2 activation. However, excessive Cu content can diminish the concentration of surface carbonaceous intermediates, thereby favor hydrogenation termination processes and suppress C–C coupling reactions. This ultimately leads to an increase in CO selectivity and a decrease in C_5^+ selectivity [16]. By precisely controlling the Cu content and distribution, an optimal catalyst (1%Na-$Cu_{0.10}FeTiO_x$) was achieved, demonstrating selectivity of 28.0% (26.9%) for alcohols (higher alcohols). Furthermore, the enhancement in the selectivity for alcohols (from 16.4% to 28.0%) and higher alcohols (from 16.1% to 26.9%), and in the STY (from 79.4 $g{\cdot}kg_{cat}^{-1}{\cdot}h^{-1}$ to 118.4 $g{\cdot}kg_{cat}^{-1}{\cdot}h^{-1}$) of higher alcohols, are illustrated in Figures 1b and Figures 1c.

The space velocity of 1%Na-$Cu_{0.10}FeTiO_x$ was further adjusted to enhance the STY of higher alcohols. As shown in Figure 1d, the catalytic performance of 1%Na-$Cu_{0.10}FeTiO_x$ for CO_2 decreases with increasing space velocity, which is attributed to the reduced residence time of CO_2 on the catalyst surface. Concurrently, the selectivity for CO increases, indicating that higher space velocities facilitate the desorption of CO. Interestingly, the 1%Na-$Cu_{0.10}FeTiO_x$ catalyst maintains a high selectivity for higher alcohols up to a space velocity of 8000 mL $g_{cat}^{-1}·h^{-1}$ (Figure 1e). However, further increases in space velocity result in a decline in the selectivity for higher alcohols. This reduction is attributed to the suppression of coupling between alkyl species and C(H)O* intermediates at elevated space velocities, leading to an increased formation of C_1-C_5 hydrocarbon products [22]. These findings are in complete agreement with the results presented in Figure 1d and Supplementary Table 2.

The effect of temperature on the thermodynamic equilibrium of CO_2 hydrogenation to higher alcohols was investigated by systematically adjusting the reaction temperature. As shown in Supplementary Figure 1, an increase in temperature (below 340°C) leads to a corresponding enhancement in the selectivity towards alcohols, with a notable increase in the selectivity for higher alcohols as well (Supplementary Figure 2). This behavior can be attributed to the reaction is endothermic reaction, where elevated temperatures increase the equilibrium constant, thereby favoring the formation of higher alcohols. However, excessively high temperatures may lead to increase side reactions, such as methane formation, thereby reducing the selectivity of alcohols and higher alcohols. These results indicate that the thermodynamic equilibrium constant for CO_2 hydrogenation to higher alcohols using a 1%Na-$Cu_{0.10}FeTiO_x$ catalyst reaches an optimal value at 340 °C. Importantly, the thermodynamic equilibrium of the CO_2 hydrogenation reaction is also reflected in these findings. According to the principles of chemical equilibrium, increasing the temperature favors the forward reaction of the reverse water-gas shift (RWGS) reaction, thus facilitating the conversion of CO_2 to CO. Consequently, with rising temperature, the CO_2 conversion rate increases dramatically (from 18.4% at 300 °C to 48.0% at 360 °C). In summary, the enhancement of CO_2 activation and the improvement of higher alcohols selectivity significantly elevate the STY of higher alcohols (from 50.9 $g·kg_{cat}^{-1}·h^{-1}$ at 300 °C to 245.4 $g·kg_{cat}^{-1}·h^{-1}$ at 340 °C) (Supplementary Figure 3).

Active Phase

The phase structure, morphological features, elemental distribution, specific surface area, and valence-state profiles of the corresponding fresh catalysts are thoroughly characterized and description as detailed in the Supplementary Information (Supplementary Figures 4-10). Investigating the active phase of the catalyst is essential for elucidating the mechanism during the reaction process. The phase composition of the spent catalyst was analyzed using XRD. As shown in Figure 2a, the spent 1%Na-$Cu_{0.10}FeTiO_x$ catalyst is composed of Fe_3O_4, Fe_5C_2, and Cu. Notably, no metallic titanium or titanium oxide phases were detected in the spent catalyst, indicating that the form of titanium remains unaffected during the CO_2 hydrogenation catalytic process. To further elucidate the microstructure of the

spent 1%Na-$Cu_{0.10}FeTiO_x$ catalyst, the transmission electron microscopy (TEM) and high-resolution transmission electron microscopy (HRTEM) analyses were conducted. Figure 2b reveals that the spent 1%Na-$Cu_{0.10}FeTiO_x$ exhibits particles of different sizes. HRTEM results (Figure 2c) demonstrate the presence of the (311) crystal planes of Fe_3O_4, the (510) and (020) crystal planes of Fe_5C_2, and the (111) crystal plane of Cu, along with an amorphous region. Importantly, the HRTEM findings not only correlate with the phase structure observed in the XRD analysis (Figure 2a) but also suggest that the amorphous region may be attributed to the presence of metallic titanium or titanium oxides in an amorphous state.

Furthermore, the valence states and the elemental composition of the spent 1%Na-$Cu_{0.10}FeTiO_x$ catalyst were investigated using X-ray photoelectron spectroscopy (XPS). As depicted in Figure 2d, the most significant difference between the spent and fresh 1%Na-$Cu_{0.10}FeTiO_x$ catalysts is observed in the characteristic peak located around 707.77 eV, which is attributed to the presence of Fe-C chemical bonds in the spent catalyst. This formation of Fe-C bonds is a result of the carburization of elemental iron during the Fischer-Tropsch synthesis process [24-26]. The XPS fine spectrum of Ti is shown in Figure 2e. The characteristic peaks with binding energies of 457.81 eV and 463.72 eV are caused by Ti $2p_{3/2}$ and Ti $2p_{1/2}$ in the 1%Na-$Cu_{0.10}FeTiO_x$ catalyst, respectively [27, 28]. This also fully demonstrates the presence of the Ti element. Simultaneously, a notable alteration in the valence state of copper was observed (Supplementary Figure 11 and Supplementary Figure 12). Compared to the fresh 1%Na-$Cu_{0.10}FeTiO_x$ catalyst, the spent catalyst exhibited a significant decrease in the content of Cu (II) and a corresponding increase in the content of Cu (0) and Cu (I) [4, 29], attributed to the reduction processes occurring during the catalytic reaction and the CO_2-Fischer-Tropsch synthesis. Subsequently, the distribution of copper valence states was further examined using Cu LMM Auger electron spectroscopy. As shown in Figure 2f, Cu (0), Cu (I), and Cu (II) coexist in the spent catalyst, indicating a complex interplay of copper species post-reaction.

Operando Dynamic Evolution of Phase Structure and Chemical Intermediates

The operando dynamic evolution of the catalyst phase structure is crucial for identifying the active phases governing catalytic performance [30]. During the reduction and reaction processes of 1%Na-$FeTiO_x$ (Figure 3a and Figure 3b), the material initially present as Fe_2O_3 under pure H_2 (consistent with Supplementary Figure 4) first transforms into Fe_3O_4 and is ultimately reduced to metallic Fe. Upon exposure to reaction conditions, metallic Fe progressively evolves into Fe_5C_2 and Fe_3O_4, in agreement with the analysis shown in Supplementary Figure 13. These observations indicate that Fe_5C_2 and Fe_3O_4 serve as the catalytically active phases during CO_2 hydrogenation to higher alcohols. As shown in Figure 3c and Figure 3d, the phase evolution of 1%Na-$Cu_{0.1}FeTiO_x$ proceeds through distinct transformation steps. The fresh catalyst initially consists of Fe_2O_3 and CuO phases. Upon exposure to pure H_2 with increasing temperature, these phases gradually transform into Fe_3O_4, metallic Fe and a Cu_3Fe_{17} alloy, which remain stable at the end of the reduction process. This indicates that the introduction of Cu species could significantly suppress the excessive reduction of Fe species. Subsequent introduction of

CO_2/H_2 reaction conditions does not alter the phase composition, and the catalyst retains Fe_3O_4, metallic Fe and Cu_3Fe_{17}. This stability can be attributed to the relatively low pressure employed during the operando XRD testing, which is insufficient to induce carburization of metallic Fe. As evidenced by the results in Figure 2a, after the reduction and catalytic reaction processes under practical conditions, the catalyst composition consists of Fe_3O_4, metallic Cu and Fe_5C_2. These findings indicate that the presence of metallic Cu plays a crucial role as an active component in promoting selectivity toward higher alcohols.

Operando monitoring of surface intermediates provides critical insight into the mechanistic pathways of CO_2 hydrogenation toward higher alcohols. To closely approximate practical reaction conditions, the catalyst was first reduced at 400 °C under pure H_2, followed by pressurization to 5.0 MPa using He. Subsequently, the reactant gas mixture ($H_2/CO_2/Ar$ = 68/27/5) was introduced into the reactor, and the evolution of surface intermediates was operando monitored. Taking 1%Na-$FeTiO_x$ as an example (Figure 4a and Figure 4c), an intense band in the 2400-2200 cm^{-1} region was observed, which is attributed to strongly adsorbed CO_2 species on the catalyst surface. Two carbonate species were subsequently identified: monodentate carbonate (m-CO_3^{2-}: 1512, 1457, 1315 and 1289 cm^{-1}) and bidentate carbonate (b-CO_3^{2-}: 1651 and 1343 cm^{-1}) [31-33], indicating that CO_2 initially adsorbs on the catalyst surface in the form of carbonate species. These carbonates undergo stepwise hydrogenation to form bicarbonate (HCO_3^-: 1419 and 1396 cm^{-1}) [33], which is further hydrogenated to generate formate ($HCOO^-$: 1362 cm^{-1}) and CO (2183 and 2106 cm^{-1}) [31, 34, 35]. Notably, linearly adsorbed *CO species (2076 cm^{-1}) are formed [36], providing key precursors for higher alcohol synthesis via a potential CO insertion pathway. The CO species generated subsequently hydrogenated during the FTS process to produce CH_x intermediates (2934 and 3083 cm^{-1}) [36], while transiently formed CH_4 (3012 cm^{-1}) desorbs from the catalyst surface. Importantly, CO undergoes insertion into CH_3 species to form CH_3CO, which is further hydrogenated to *CH_3CHO (1749 and 1544 cm^{-1}) [18, 31]. Subsequent hydrogenation yields *CH_3CH_2O (2964 and 2878 cm^{-1}) [37], and continued hydrogenation ultimately produces $C_nH_{2n+1}OH$ and desorbs from the catalyst surface. A similar reaction pathway is observed for 1%Na-$Cu_{0.1}FeTiO_x$ during CO_2 hydrogenation to higher alcohols (Figure 4b and Figure 4d). Notably, the operando spectra of 1%Na-$Cu_{0.1}FeTiO_x$ exhibit significantly stronger characteristic bands corresponding to *CH_3CH_2O, *CO and CH_x species, which is attributed to the enhanced yield of higher alcohols during the reaction of 1%Na-$Cu_{0.1}FeTiO_x$.

Visualization Evolution Mechanism of Higher Alcohols

Based on the operando identification of active phases and surface intermediates, we propose a CO insertion mechanism for CO_2 hydrogenation to higher alcohols [11, 38-40]. The observed phase transformation from Fe_2O_3 to Fe_3O_4 and Fe_5C_2, along with the sequential formation of carbonate → *CO → *CH_x → CH_3CH_2O, provides coherent evidence for the following pathway that linearly adsorbed *CO species undergo insertion into surface alkyl intermediates, thereby enabling C-C bond formation and

subsequent hydrogenation to higher alcohol products. The hydrogenation of CO_2 to higher alcohols generally proceeds through three processes: RWGS, FTS, and CO insertion reactions (Figure 4e). Taking ethanol synthesis from CO_2 as an example, CO_2 molecules adsorbed on the catalyst surface (Fe_3O_4 phase) as monodentate or bidentate carbonates (CO_3^{2-}). Subsequently, they undergo three-step hydrogenation and deoxygenation to progressively form HCO_3^-, $HCOO^-$, and CO. The Cu species can effectively combine with the adsorbed CO. The adsorbed CO that is not transferred desorbs from the catalyst surface to form gaseous CO, most of which participates in the subsequent FTS process. Subsequently, CO was gradually hydrogenated on the catalyst surface (Fe_5C_2) to form $*CH_x$. This process is also facilitated by the influence of Na additives on Fe reduction kinetics, promoting the transformation of Fe_5C_2 and further increasing the surface coverage of $*CH_x$. At this stage, CO adsorbed on Cu sites migrates to Fe_5C_2 sites for insertion reaction, forming CH_3CO*. This species then undergoes two hydrogenation steps to sequentially form $*CH_3CHO$ and CH_3CH_2OH, with the resulting CH_3CH_2OH desorbing from the catalyst surface.

Conclusion

In summary, we report a titanium iron ore material $FeTiO_x$ containing amorphous Ti species synthesized via a high-temperature calcination strategy for selective higher alcohols synthesis. Under the regulation of the electronic aid Na, the $FeTiO_x$ framework exhibits an intrinsic preference for alcohol formation, while adjusting the dispersion of Cu species further enhances higher alcohols selectivity to 31.1%, while maintaining a CO_2 conversion rate of 42.5%, highlighting the critical role of surface Cu sites in regulating catalytic behavior. The operando X-ray diffraction (XRD) and operando DRIFTS results reveal the dynamic evolution of catalyst phases (formation of a Fe_3O_4/Fe_5C_2/Cu interface) and surface intermediates (carbonate → $*CO$ → $*CH_x$ → CH_3CH_2O) during the catalytic reaction. These observations provide direct insight into the structure-reactivity relationship governing alcohol formation. This study offers mechanistic understanding of Fe-based perovskite catalysts and establishes a viable strategy for designing efficient catalytic systems for the selective production of higher alcohols from carbon-based feedstocks.

Declarations

Author contributions

Teng Li: Conceptualization, methodology, investigation, data curation, formal analysis, result discussion, writing-original draft and writing-review and editing. **Lijun Zhang:** Result discussion and formal analysis. **Zhenkun Liu, Jiaming Liang, Hao Chen, Linlin Zhao, Shunnosuke Fujii, Peng Qin, Qiang Liu, Tao Li, Tao Xing, Jiancai Sui** and **Yongqiang Gu:** Investigation and formal analysis. **Zhiliang Jin** and **Noritatsu Tsubaki:** Data curation, methodology, resources, project administration, supervision, and writing-review and editing.

Conflicts of interest

The authors declare that they have no competing interests.

Acknowledgements

This work was financially supported by the NEDO of Japan, the National Natural Science Foundation of China (22408001), the Ningxia Hui Autonomous Region Natural Science Foundation Project (2023AAC02046), China Scholarship Council (CSC, 202408050073), the Grant-in-Aid from Japan Society for the Promotion of Science (JSPS) (22H01864, 23H05404).

References

1. Lijun Zhang, Teng Li, Wenjie Xiang, Zhiwei Ye, Luyao Wu, Wei Xia, Hao Huang, Zhihao Liu, Xiuyun Jiang, Guangbo Liu, Zhiliang Jin, Weizhe Gao, Hongliang Li, Jie Zeng, Noritatsu Tsubaki, Direct Synthesis of para-Xylene from CO_2 Hydrogenation with a Record-High Space-Time Yield, ***Journal of the American Chemical Society***, 147, 28, 2025, 24442-24450.
2. Teng Li, Xuanpu Wang, Zhiliang Jin, Noritatsu Tsubaki, Tailoring Advanced CdS Anisotropy-Driven Charge Spatial Vectorial Separation and Migration via In Situ Dual Co-Catalyst Synergistic Layout, ***Small***, 20, 31, 2024, 2311441.
3. Xiaohui Feng, Haoran Jia, Rongtan Li, Le Lin, Mingrun Li, Mingshu Chen, Chengxiang Liu, Xiangze Du, Xiaoyue Wang, Yunjie Ding, Rentao Mu, Qiang Fu, Xinhe Bao, ZnO_x overlayer confined on $ZnCr_2O_4$ spinel for direct syngas conversion to light olefins, ***Nature Communications***, 16, 2025, 3711.
4. Cheng Yang, Xuanpu Wang, Teng Li, Youlin Wu, Zhiliang Jin, Rational Design and Construction of Graphdiyne (C_nH_{2n-2}) Based $NiMoO_4$/GDY/CuO in Situ XPS Proved Double S-Scheme Heterojunctions for Photocatalytic Hydrogen Production, ***Langmuir***, 39, 28, 2023, 9816-9830.
5. Yi Cai, Maolin Wang, Shu Zhao, Xi Liu, Junzhong Xie, Xing-Wu Liu, Yao Xu, Jie Zhang, Lingzhen Zeng, Fei Qian, Zirui Gao, Zeyan Cen, Xingchen Liu, Hong Wang, Bingjun Xu, Graham J. Hutchings, Yong Yang, Yong-Wang Li, Xiao-Dong Wen, Ding Ma, Trace-level halogen blocks CO_2 emission in Fischer-Tropsch synthesis for olefins production, ***Science***, 390, 2025, 516-520.
6. Yang Cheng, Shujing Li, Han Li, Di Meng, Shuxian Zhang, Ming Qing, Min Pan, Fuyun Yang, Chengwei Wang, Lei Li, Guangbo Liu, Peng Qin, Chufeng Liu, Hanyao Song, Haozhe Feng, Hao Chen, Jifan Li, Chun-Ling Liu, Noritatsu Tsubaki, Wen-Sheng Dong, $CuFeO_2$ Integrated with Orderly Stacked Multilamellar ZSM-5 Nanosheets for Highly Active and Selective Synthesis of Aromatics from CO_2 Hydrogenation, ***ACS Catalysis***, 15, 17, 2025, 15706-15721.
7. Jie Tuo, Zhenteng Sheng, Xianchen Gong, Qi Yang, Peng Wu, Hao Xu, Shape-selective synthesis of para-xylene through tandem CO_2 hydrogenation and toluene methylation over $ZnCeZrO_x$/MCM-22 catalyst, ***Chinese Journal of Catalysis***, 73, 2025, 174-185.

8. Mingrui Wang, Shendong Guo, Siyang Yan, Zhiqun Wang, Guanghui Zhang, Hui Gao, Miao Zhang, Kai Bian, Jiaxu Liu, Xiaowa Nie, Jianrong Zeng, Chunshan Song, Xinwen Guo, Engineering the Cu(0)-Co_2C Interface via Reaction-Induced Reconstruction for CO_2 Hydrogenation to C_2^+ Hydrocarbons, ***Journal of the American Chemical Society***, 147, 45, 2025, 42051-42060.
9. Jiaming Liang, Lei Jiang, Hengyang Liu, Bowei Meng, Zhiliang Jin, Lisheng Guo, Zhihao Liu, Teng Li, Wenhang Wang, Chengwei Wang, Ying Shi, Guangbo Liu, Kai Sun, Yingluo He, Bing Liang, Noritatsu Tsubaki, Engineering Interfacial Oxygen Vacancies of Zn-Cr Sites for CO_2 Activation and Hydrogenation, ***ACS Catalysis***, 15, 9, 2025, 7340-7350.
10. Bowei Meng, Jiaming Liang, Lei Jiang, Miaohui Song, Bowen Jian, Zhihao Liu, Teng Li, Baojian Chen, Chufeng Liu, Hanyao Song, Peipei Zhang, Guangbo Liu, Jiancai Sui, Qiang Liu, Tao Li, Tao Xing, Dingcheng Liang, Bing Liang, Noritatsu Tsubaki, Efficient Production of Liquefied Petroleum Gas from CO_2 Hydrogenation by Combining Fe-Al Bimetallic Catalyst with SSZ-13 Zeolite, ***ACS Catalysis***, 15, 21, 2025, 17991-18003.
11. Yang Chen, Diwen Zhou, Yongli Chang, Yunzhao Xu, Hongqiao Lin, Lizhi Wu, Yu Tang, Chengyi Dai, Xingang Li, Lisheng Guo, Ting Qiu, Li Tan, Rh-Based Bimetallic Alloys: Unraveling the Synergistic Catalysis in CO_2 Hydrogenation to Ethanol, ***ACS Catalysis***, 15, 12, 2025, 10068-10081.
12. Wenhang Wang, Xiangyu Guo, Yang Wang, Simin Lin, Xinhua Gao, Jie Liang, Jinqiang Zhang, Jinghao Xie, Hu Jiang, Fengliang Cao, Yongjie Chen, Guohui Yang, Thomas Frauenheim, Mingqing Wang, Tao Xing, Yiwu Lu, Qiang Liu, Kostya S. Novoselov, Noritatsu Tsubaki, Mingbo Wu, Transformation of CO_2 to C_2^+ alcohols by tailoring the oxygen bonding via Fe-based tandem catalyst, ***Nature Communications***, 16, 2025, 7265.
13. Lijun Zhang, Mengying Du, Teng Li, Fan Huang, Chenchen Cai, Haitao Wu, Caixia Zhu, Prasert Reubroycharoen, Guangbo Liu, Wei Xia, Mingbo Wu, Noritatsu Tsubaki, Rational catalyst customization for the targeted valorization of CO_2 into aromatics, ***Chemical Engineering Journal***, 529, 2026, 172785.
14. Haiyan Yang, Zhangqian Wei, Jian Zhang, Yaru Dang, Shenggang Li, Xianni Bu, Zixuan Zhou, Chenfan Gong, Hao Wang, Jiong Li, Yang Liu, Yong Yang, Tianci Xiao, Chengyuan Liu, Yuhan Sun, Peng Gao, Tuning the selectivity of CO_2 hydrogenation to alcohols by crystal structure engineering, ***Chem***, 10, 7, 2024, 2245-2265.
15. Shican Jiang, Xuan Gong, Xinyu You, Xin Zhang, Yining Li, Abhishek Dutta Chowdhury, Investigating the Catalytic Impact of Iron-Based Metal-Organic Framework Templates on the CO_2-Derived Fischer-Tropsch Synthesis Process, ***CCS Chemistry***, 6, 2024, 2908-2925.
16. Ruwei Yao, Yang Yu, Bin Wu, Yueyin Song, Qinqin Niu, Congming Li, Jian Wei, Qingjie Ge, Synergistic Na-S modified Fe-Cu catalysts for efficient CO_2 hydrogenation to higher alcohols, ***Chemical Engineering Journal***, 512, 2025, 162498.
17. Yuzhen Ge, Antonio J. Martín, Manu Suvarna, Tangsheng Zou, Frank Krumeich, Javier Pérez-Ramírez, Descriptors toward higher alcohols and olefins formation in CO_2 hydrogenation on promoted iron

catalysts, ***Applied Catalysis B: Environment and Energy***, 378, 2025, 125578.

18. Qian Zhang, Sen Wang, Rui Geng, Pengfei Wang, Mei Dong, Jianguo Wang, Weibin Fan, Hydrogenation of CO_2 to higher alcohols on an efficient Cr-modified CuFe catalyst, ***Applied Catalysis B: Environment and Energy***, 337, 2023, 123013.
19. Ruwei Yao, Jian Wei, Qingjie Ge, Jing Xu, Yu Han, Qingxiang Ma, Hengyong Xu, Jian Sun, Monometallic iron catalysts with synergistic Na and S for higher alcohols synthesis via CO_2 hydrogenation, ***Applied Catalysis B: Environment and Energy***, 298, 2021, 120556.
20. Baojian Chen, Caixia Zhu, Haozhe Feng, Teng Li, Zhihao Liu, Zhenzhou Zhang, Yingluo He, Noritatsu Tsubaki, Enhancing higher alcohols selectivity in CO_2 hydrogenation over FeCu catalysts via Mg modification, ***Catalysis Today***, 463, 2026, 115614.
21. Yang Wang, Kangzhou Wang, Baizhang Zhang, Xiaobo Peng, Xinhua Gao, Guohui Yang, Han Hu, Mingbo Wu, Noritatsu Tsubaki, Direct Conversion of CO_2 to Ethanol Boosted by Intimacy-Sensitive Multifunctional Catalysts, ***ACS Catalysis***, 11, 18, 2021, 11742-11753.
22. Yuling Ma, Shuang Liu, Xin Han, Lei Ye, Haitao Xu, Lingtao Kong, Jiangbing Li, Xin Pu, Jichang Liu, Efficient Hydrogenation of CO_2 to Higher Alcohols over Cu–Zn–Fe Catalysts: The Role of ZnFe2O4 Spinel Precursor, ***ACS Sustainable Chemistry & Engineering***, 14, 2026, 1467–1476.
23. Di Xu, Yanqiu Wang, Mingyue Ding, Xinlin Hong, Guoliang Liu, Shik Chi Edman Tsang, Advances in higher alcohol synthesis from CO_2 hydrogenation, ***Chem***, 7, 4, 2021, 849-881.
24. Lijun Zhang, Jiankang Zhao, Teng Li, Weizhe Gao, Hongliang Li, Luyao Wu, Wei Xia, Wenlong Wu, Chengwei Wang, Fan Wang, Shuhei Yasuda, Xiaoyu Guo, Yingluo He, Guohui Yang, Guangbo Liu, Zhiliang Jin, Jie Zeng, Noritatsu Tsubaki, Long-Term CO_2 Hydrogenation into Liquid Fuels with a Record-High Single-Pass Yield of 31.7% over Interfacial Fe-Zn Sites, ***Nano Letters***, 25, 2025, 4904-4912.
25. Teng Li, Heng Zhao, Lisheng Guo, Guangbo Liu, Jinhu Wu, Tao Xing, Tao Li, Qiang Liu, Jiancai Sui, Yitong Han, Jiaming Liang, Yingluo He, Noritatsu Tsubaki, Construction of Highly Active Fe_5C_2-FeCo Interfacial Sites for Oriented Synthesis of Light Olefins from CO_2 Hydrogenation, ***ACS Catalysis***, 15, 2025, 1112-1122.
26. Teng Li, Lijun Zhang, Jiaming Liang, Yitong Han, Zhihao Liu, Jiancai Sui, Qiang Liu, Tao Li, Tao Xing, Guangbo Liu, Peipei Zhang, Xiaobo Feng, Zhiliang Jin, Noritatsu Tsubaki, FeCo Alloy Clusters Optimized Heterogeneous Catalytic Interface for Driving CO_2 Hydrogenation to Light Olefins, ***Advanced Functional Materials***, 35, 2025, 2505432.
27. Aiyun Meng, Shuang Zhou, Da Wen, Peigang Han, Yaorong Su, g-C_3N_4/$CoTiO_3$ S-scheme heterojunction for enhanced visible light hydrogen production through photocatalytic pure water splitting, ***Chinese Journal of Catalysis***, 43, 2022, 2548-2557.
28. Teng Li, Xuanpu Wang, Zhiliang Jin, Noritatsu Tsubaki, Enhanced kinetics of photocatalytic hydrogen evolution by interfacial Co-C bonded strongly coupled S-scheme inorganic perovskite/organic graphdiyne (C_nH_{2n-2}) heterojunction, ***Chemical Engineering Journal***, 477, 2023, 147018.

29. Zhiliang Jin, Xuanpu Wang, Youlin Wu, Teng Li, Graphdiyne (C_nH_{2n-2}) based S-scheme heterojunction to promote carrier transfer for efficiently photocatalytic hydrogen evolution, ***2D Materials***, 10, 2023, 025022.
30. Ayaka Miura, Teng Li, Lijun Zhang, Jiaming Liang, Yitong Han, Hao Huang, Baojian Chen, Zhenkun Liu, Peng Qin, Kenji Nakao, Noriyuki Yamaneb, Caixia Zhu, Guangbo Liu, Prasert Reubroycharoen, Yingluo He, Zhiliang Jin, Mingbo Wu, Noritatsu Tsubaki, High-Yield Production of Light Olefins from CO_2 Hydrogenation over Co-Promoted Na-FeMn Catalysts, ***ACS Catalysis***, 2026, https://doi.org/10.1021/acscatal.6c00962.
31. Ruwei Yao, Bin Wu, Yang Yu, Na Liu, Qinqin Niu, Congming Li, Jian Wei, Qingjie Ge, Regulating the electronic property of iron catalysts for higher alcohols synthesis from CO_2 hydrogenation, ***Applied Catalysis B: Environment and Energy***, 355, 2024, 124159.
32. Qixin Fan, Na Liu, Jingming Zhao, Yang Yu, Yannan Sun, Yu Han, Jixin Zhang, Aimin Wang, Qingjie Ge, Jian Wei, Jian Sun, Regulating the location of metal promoters in CuFe-based catalysts for enhanced CO_2 hydrogenation to higher alcohols, ***Journal of Energy Chemistry***, 107, 2025, 31-43.
33. Tingmin Di, Bicheng Zhu, Bei Cheng, Jiaguo Yu, Jingsan Xu, A direct Z-scheme g-C_3N_4/SnS_2 photocatalyst with superior visible-light CO_2 reduction performance, ***Journal of Catalysis***, 352, 2017, 532-541.
34. Yanqiu Wang, Xinxin Zhang, Xinlin Hong, Guoliang Liu, Sulfate-Promoted Higher Alcohol Synthesis from CO_2 Hydrogenation, ***ACS Sustainable Chemistry & Engineering***, 10, 27, 2022, 8980-8987.
35. Qian Zhang, Sen Wang, Xuerong Shi, Mei Dong, Jiangang Chen, Juan Zhang, Jianguo Wang, Weibin Fan, Conversion of CO_2 to higher alcohols on K-CuZnAl/Zr-CuFe composite, ***Applied Catalysis B: Environment and Energy***, 346, 2024, 123748.
36. Xiaomeng Yuwen, Xiaoliang Mu, Lu Zhao, Kegong Fang, Induced ethanol and higher alcohols formation during CO hydrogenation over a novel MoS_2-MoO_3 composite catalyst, ***Chemical Engineering Journal***, 525, 2025, 170276.
37. Di Xu, Hengquan Yang, Xinlin Hong, Guoliang Liu, Shik Chi Edman Tsang, Tandem Catalysis of Direct CO_2 Hydrogenation to Higher Alcohols, ***ACS Catalysis***, 11, 15, 2021, 8978-8984.
38. Andrii Kostyniuk, Blaž Likozar, High-yield ethanol production via thermocatalytic CO_2 hydrogenation over Cs/CuZnFe catalyst in a continuous flow reactor, ***Chemical Engineering Journal***, 520, 2025, 166135.
39. Yang Wang, Wenhang Wang, Ruosong He, Meng Li, Jinqiang Zhang, Fengliang Cao, Jianxin Liu, Shiyuan Lin, Xinhua Gao, Guohui Yang, Mingqing Wang, Tao Xing, Tao Liu, Qiang Liu, Han Hu, Noritatsu Tsubaki, Mingbo Wu, Carbon-Based Electron Buffer Layer on ZnO_x-Fe_5C_2-Fe_3O_4 Boosts Ethanol Synthesis from CO_2 Hydrogenation, ***Angewandte Chemie International Edition***, 62, 46, 2023, e202311786.
40. Shiquan Huang, Ling Fang, Siling Luo, Hao Deng, Tomas Ramirez Reina, Guangting Zou, Qing Liu, Rongbin Zhang, Maohong Fan, Jinshu Tian, Gang Feng, Runping Ye, Tailoring electronic and

interfacial synergy in Cu-FeGa/Al_2O_3 for direct CO_2 hydrogenation to ethanol, ***Chemical Engineering Journal***, 531, 2026, 173969.

Figures

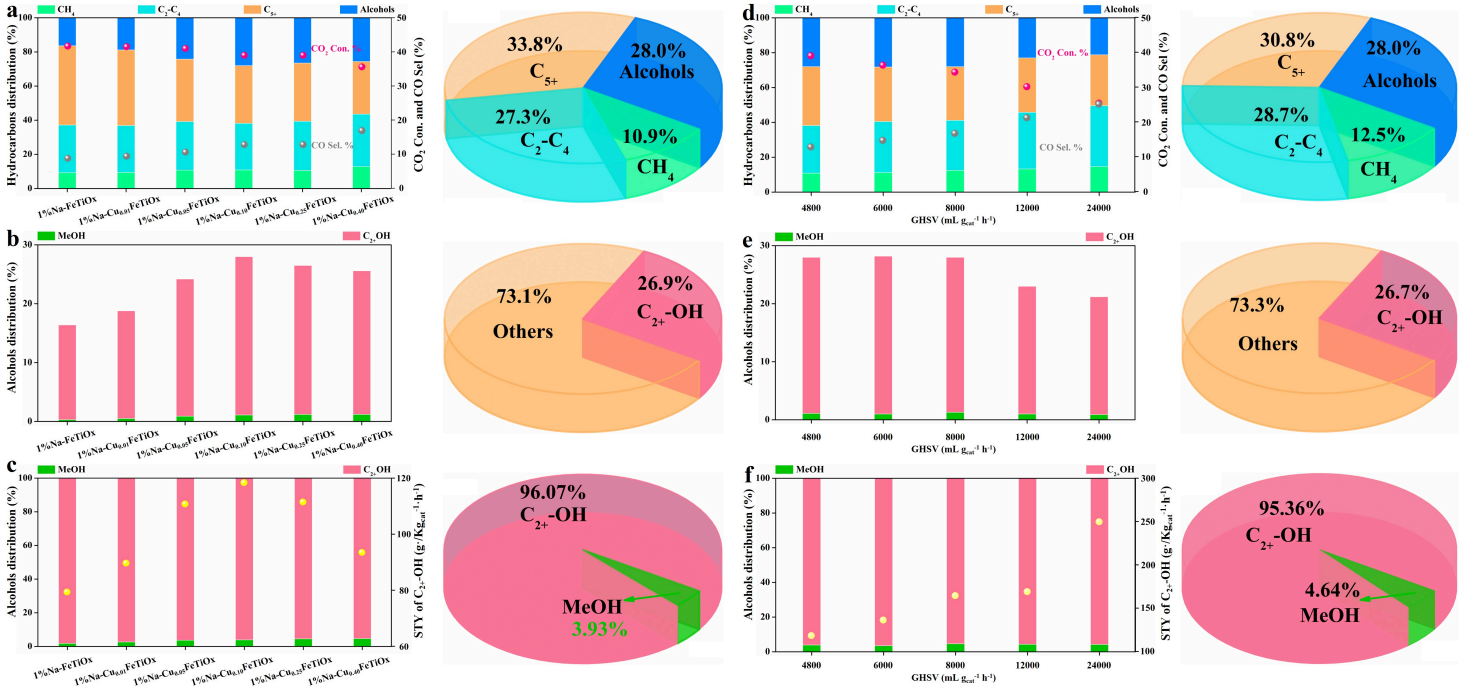

Figure 1

Catalytic activity of CO_2 hydrogenation. a CO_2 hydrogenation performance of different Fe-based catalysts (Pie chart: Product distribution of 1%Na-$Cu_{0.10}FeTiO_x$). **b** Alcohols distribution of different Fe-based catalysts (Pie chart: Alcohol distribution of 1%Na-$Cu_{0.10}FeTiO_x$). **c** Percentage of higher alcohols in the alcohol and the STY of higher alcohols for different iron-based catalysts (Pie chart: Alcohol phase distribution of 1%Na-$Cu_{0.10}FeTiO_x$). Reaction conditions (**a-c**): 5.0 MPa, 320 °C, CO_2: H_2 =1:2.5, GHSV = 4800 mL g_{cat}^{-1} h^{-1}. **d** CO_2 hydrogenation performance of 1% Na-$Cu_{0.10}FeTiO_x$ under different GHSV (Pie chart: Product distribution of 1%Na-$Cu_{0.10}FeTiO_x$ under GHSV=8000 mL g_{cat}^{-1} h^{-1}). **e** Alcohol distribution of 1% Na-$Cu_{0.10}FeTiO_x$ under different GHSV (Pie chart: Alcohol distribution of 1%Na-$Cu_{0.10}FeTiO_x$ under GHSV=8000 mL g_{cat}^{-1} h^{-1}). **f** Percentage of higher alcohols in the alcohol and the STY of higher alcohols for 1% Na-$Cu_{0.10}FeTiO_x$ under different GHSV (Pie chart: Alcohol phase distribution of 1%Na-$Cu_{0.10}FeTiO_x$ under GHSV=8000 mL g_{cat}^{-1} h^{-1}). Reaction conditions (d-f): 5.0 MPa, 320 °C, CO_2: H_2 =1:2.5.

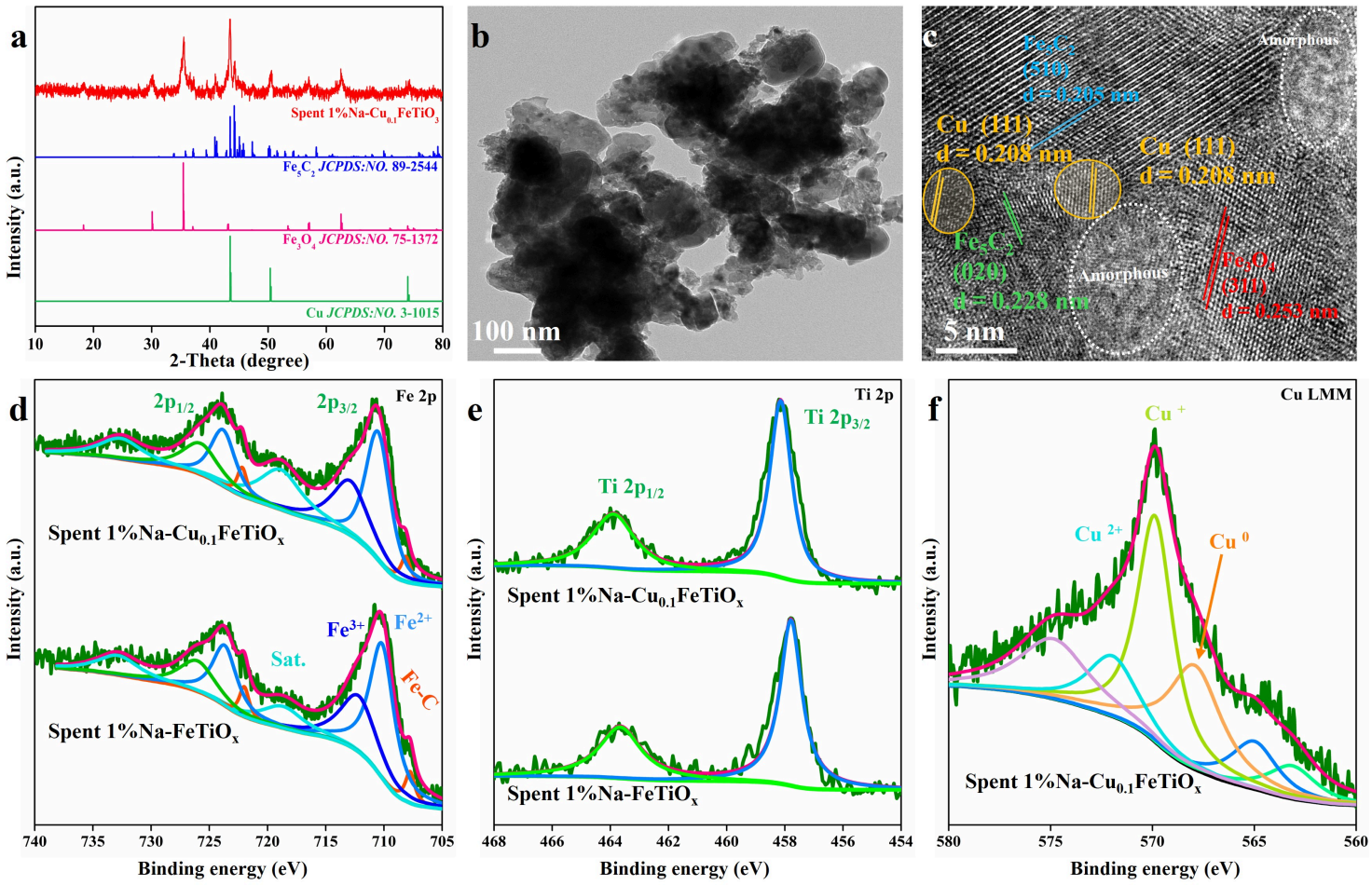

Figure 2

Active phase of catalysts. a XRD patterns of spent 1%Na-$Cu_{0.10}FeTiO_x$. **b** TEM patterns of spent 1%Na-$Cu_{0.10}FeTiO_x$. **c** HRTEM of spent 1%Na-$Cu_{0.10}FeTiO_x$. **d** Fe 2p XPS fine spectra of spent 1%Na-$FeTiO_x$ and spent 1%Na-$Cu_{0.10}FeTiO_x$. **e** Ti 2p XPS fine spectra of spent 1%Na-$FeTiO_x$ and spent 1%Na-$Cu_{0.10}FeTiO_x$. **f** Cu LMM XPS fine spectra of spent 1%Na-$Cu_{0.10}FeTiO_x$.

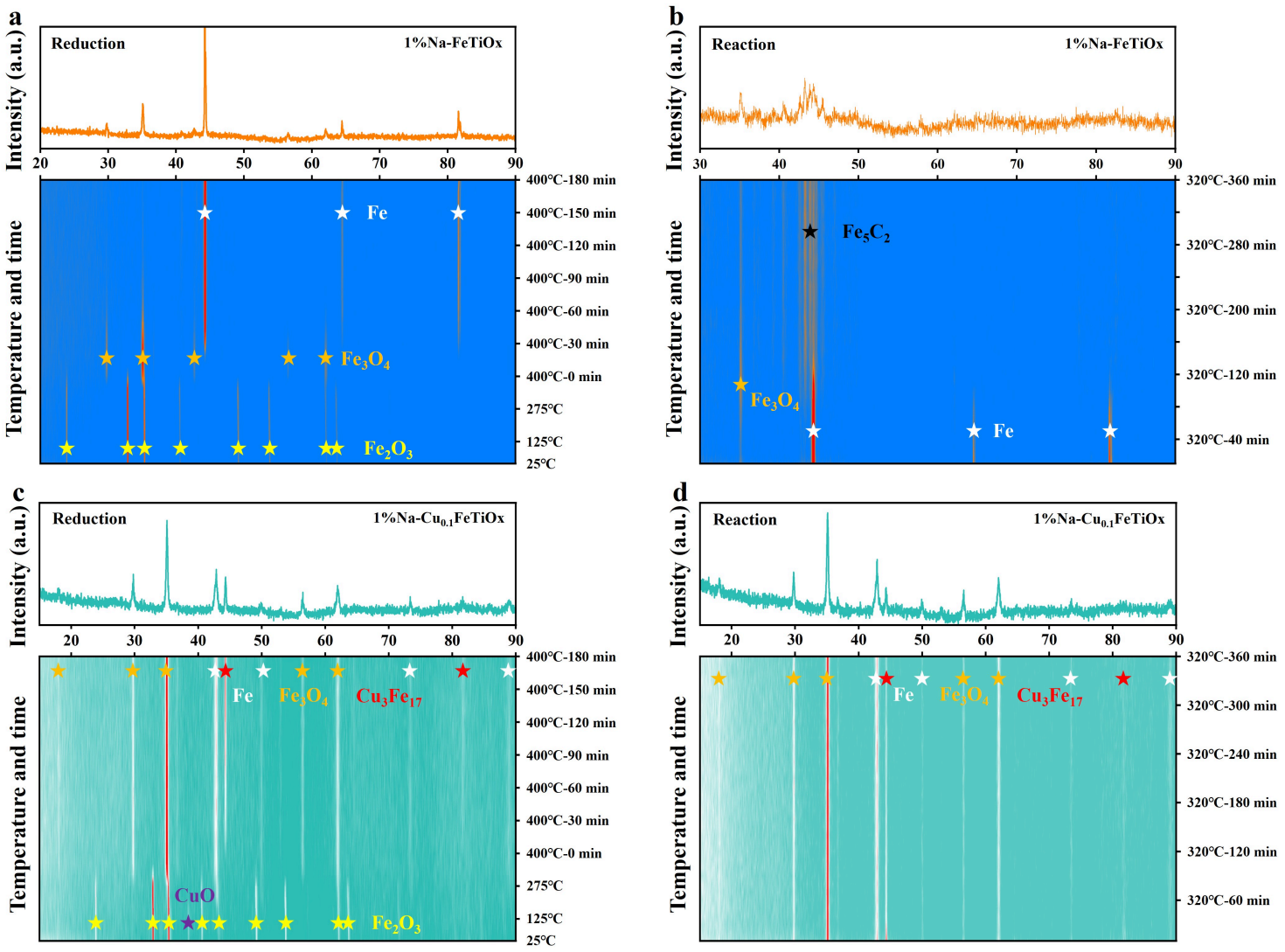

Figure 3

Operando Dynamic Evolution of Phase Structure. a Operando XRD patterns of 1%Na-FeTiO$_x$ during reduction process. **b** Operando XRD patterns of 1%Na-FeTiO$_x$ during reaction process. **c** Operando XRD patterns of 1%Na-Cu$_{0.1}$FeTiO$_x$ during reduction process. **d** Operando XRD patterns of 1%Na-Cu$_{0.1}$FeTiO$_x$ during reaction process. Reduction conditions: Atmospheric pressure, 25-400 °C, Hydrogen flow rate is 40 mL/min. Reaction conditions: Atmospheric pressure, 320 °C, $H_2/CO_2/Ar$ = 68%/27%/5%, Feed gas flow rate is 20 mL/min.

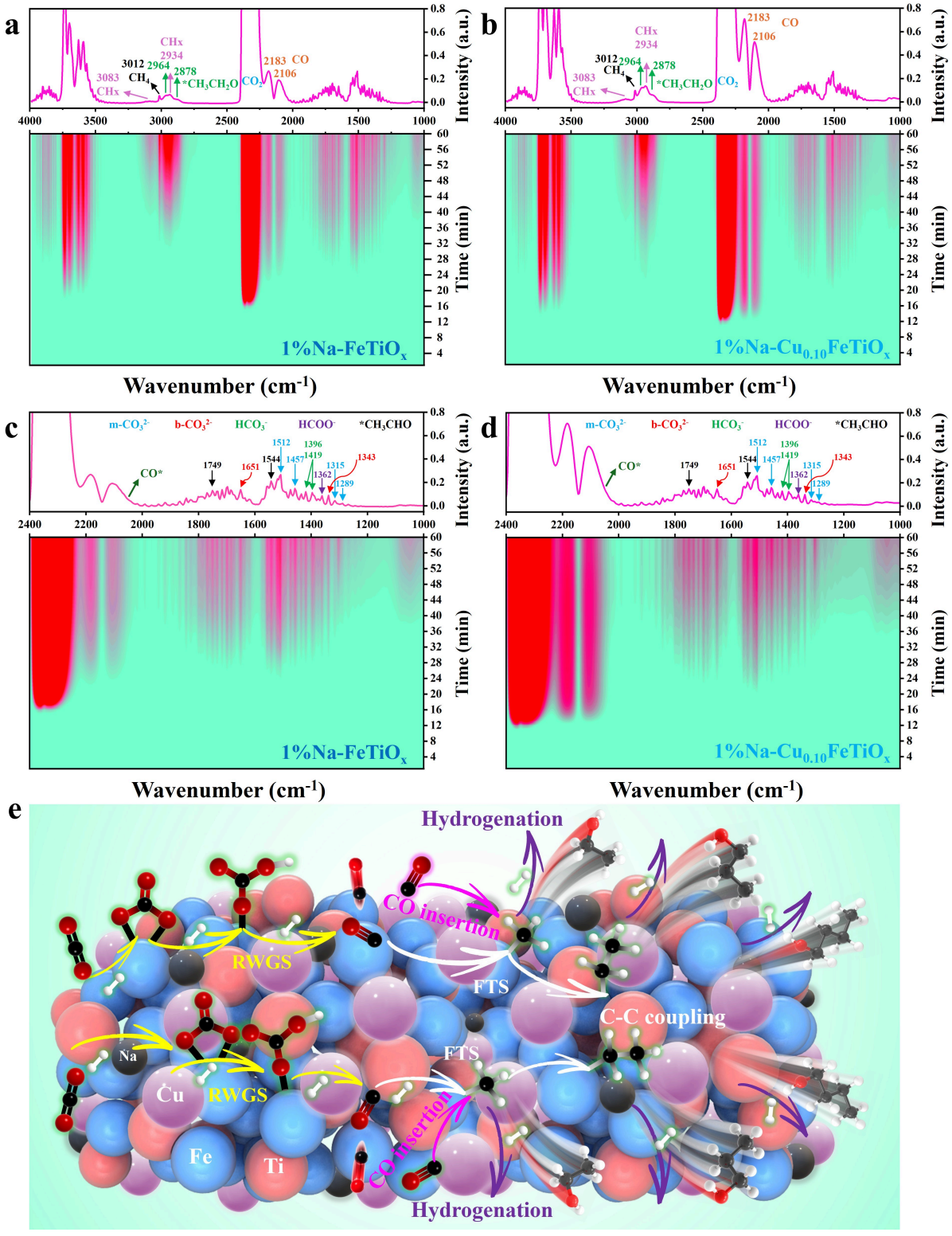

Figure 4

Operando Dynamic Evolution of Chemical Intermediates. a, b Operando DRIFT spectroscopy during the CO_2 hydrogenation of 1%Na-$FeTiO_x$. **c, d** Operando DRIFT spectra during the CO_2 hydrogenation of 1%Na-$Cu_{0.10}FeTiO_x$. Reduction conditions: Atmospheric pressure, 25-400 °C, Hydrogen flow rate is 60 mL/min.

Reaction conditions: 5.0 MPa, 320 °C, $H_2/CO_2/Ar$ = 68%/27%/5%, Feed gas flow rate is 20 mL/min. **e** Visualization evolution of higher alcohols from CO_2 hydrogenation over 1%Na-$Cu_{0.10}FeTiO_x$.

Supplementary Files

This is a list of supplementary files associated with this preprint. Click to download.

- SupportingInformation.docx
- image5.tif